phycology

IMPACT FACTOR 2.9

CITESCORE 5.2

Article

Removal of Fluoride from Aqueous Solution Using Biochar Derived from Brown Macroalgae (*Sargassum Polycystum*) Impregnated with Fe_3O_4 Nanoparticles

Sania Kanwal, Satesh Kumar Devrajani and Saif Ali Khan Hashmani

MDPI

https://doi.org/10.3390/phycology5030037

phycology

MDPI

Article

Removal of Fluoride from Aqueous Solution Using Biochar Derived from Brown Macroalgae (*Sargassum Polycystum*) Impregnated with Fe_3O_4 Nanoparticles

Sania Kanwal [1], Satesh Kumar Devrajani [2,*] and Saif Ali Khan Hashmani [3]

[1] Department of Civil, Environmental, and Architectural Engineering, University of Padova, Via 8 Febbraio, 2, 35122 Padova, Italy
[2] Department of Civil, Environmental, Architectural Engineering and Mathematics, University of Brescia, Via Branze 43, 25123 Brescia, Italy
[3] Department of Energy and Environment, Faculty of Agricultural Engineering, Sindh Agriculture University, TandoJam 70060, Pakistan
* Correspondence: satesh086@outlook.com

Abstract

This study explores the enhancement of fluoride adsorption using biochar derived from the brown macroalga *Sargassum polycystum*, which was treated with iron oxide (Fe_3O_4). The macroalgal biomass underwent pyrolysis at 400 °C, followed by Fe_3O_4 impregnation, to improve surface functionality and create active sites for fluoride ion binding. Various factors affecting fluoride removal were systematically examined. A maximum fluoride removal effectiveness of 90.2% was attained under ideal circumstances (pH 2, 60 mg adsorbent dose, 30 mg/L fluoride concentration, and 150 min contact duration). Adsorption isotherm analysis showed that the Langmuir model provided a better fit (R^2 = 0.998) than the Freundlich model (R^2 = 0.941), with a maximum adsorption capacity (q_m) of 3.41 mg/g, indicating monolayer adsorption on a homogeneous surface. Kinetic modeling revealed that the pseudo-second-order model best described the adsorption process (R^2 = 0.9943), suggesting chemisorption as the dominant mechanism, while the intraparticle diffusion model also showed a good fit (R^2 = 0.9524), implying its role in the rate-limiting step. Surface complexation, facilitated by the enhanced surface area and porosity of the iron-modified biochar, was identified as the primary mechanism of fluoride ion interaction. This study highlights the potential of Fe_3O_4-modified macroalgal biochar as an effective and sustainable solution for fluoride remediation in contaminated water sources.

Keywords: fluoride; Fe_3O_4; water treatment; brown macroalgae; biochar; adsorption kinetics

Academic Editor: Marcin Dębowski

Received: 13 July 2025
Revised: 5 August 2025
Accepted: 9 August 2025
Published: 13 August 2025

Citation: Kanwal, S.; Devrajani, S.K.; Hashmani, S.A.K. Removal of Fluoride from Aqueous Solution Using Biochar Derived from Brown Macroalgae (*Sargassum Polycystum*) Impregnated with Fe_3O_4 Nanoparticles. *Phycology* **2025**, *5*, 37. https://doi.org/10.3390/phycology5030037

1. Introduction

Groundwater is the most abundant and accessible source of freshwater globally and remains vital for meeting the increasing demands of human consumption, agriculture, and industrial activities [1]. However, groundwater contamination by fluoride has emerged as a significant environmental and public health challenge. Fluoride, a naturally occurring anion, is primarily introduced into the environment through the weathering of fluoride-containing minerals [2]. Additionally, industrial processes, including semiconductor manufacturing, electroplating, glass production, steelmaking, cement manufacturing, aluminum smelting, ceramics, and fertilizer production, contribute substantially to fluoride contamination through the discharge of wastewater and surface runoff [3]. This contamination is

particularly concerning in arid and semi-arid regions, where groundwater serves as the primary drinking water source [4,5].

The WHO has established fluoride limits in drinking water at 0.5–1.5 mg/L [6]. Levels exceeding these thresholds can result in severe health issues, including dental and skeletal fluorosis, particularly with prolonged exposure [4,5]. In rural areas of developing nations such as Pakistan, India, Africa, and China, contamination of fluoride in groundwater has caused socio-economic disruptions, including the abandonment of contaminated bore wells and adverse health impacts on affected populations [4,5,7,8].

Various remediation technologies for water treatment, including precipitation, ion exchange, membrane separation, reverse osmosis, flocculation, nanofiltration, and electro-coagulation chemical treatments, have been used [9–15]. However, these techniques are costly and create toxicity at the end of the process. Nonetheless, the limitations associated with many of these approaches encompass elevated operational and maintenance expenses, the potential for secondary contamination (such as the production of hazardous sludge), and the intricate nature of the treatment procedures.

However, among them, adsorption has emerged as a widely used, efficient, and cost-effective technique for fluoride removal [10,16]. Additionally, the use of biochar for adsorption has grown in popularity because of its simple, affordable, and self-renewing qualities. Organic matter is pyrolyzed to create biochar, a porous, carbon-rich substance that has shown promise as an affordable, environmentally safe, and effective adsorbent for eliminating pollutants from water [17,18]. Its physicochemical properties are influenced by feedstock characteristics such as elemental composition, density, and ash content, as well as pyrolysis conditions like temperature [19–21]. Recent investigations have demonstrated the potential of adsorbents derived from different feedstocks, including corn stovers, pine wood, and rice husk, for fluoride removal under specific conditions [21–23]. However, the research on the application of macroalgae (brown seaweed)-derived iron-modified biochar for fluoride removal is currently unexplored.

Coastal regions and water bodies are home to a variety of algae species known as "seaweed/macroalgae," which play vital functions as food sources and possible habitats for a variety of marine organisms [24,25]. In many countries, such as Vietnam, China, South Korea, and Singapore, macroalgae are used as potential habitats, food, and pharmaceuticals. Beyond their versatile applications, they can also be considered for the preparation of adsorbents for adsorption purposes. Because of this potential, macroalgae present a viable and sustainable solution for problems related to water treatment and other industrial uses [25,26]. Commercial adsorbents/biochar are used to remove contaminants, but their efficacy in removing fluoride has not yet been determined. This has been addressed by impregnating or surface-modifying biochar made from seaweed to improve its adsorption capabilities for eliminating contaminants, such as fluoride.

Brown macroalgae possess several distinct compositional and structural advantages. First, they are rich in polysaccharides (e.g., alginate and fucoidan), which upon pyrolysis yield biochar with higher oxygen-containing functional groups (e.g., -COOH and -OH), enhancing ion-exchange capacity and surface reactivity for anion adsorption such as fluoride [24,26–28]. Second, their cell wall structure is more porous and less lignified than terrestrial biomass, which facilitates the development of higher surface area and porosity during pyrolysis [27,29]. For instance, biochar derived from *Sargassum* spp. has been reported to exhibit higher ash content (up to 30–40%) rich in Ca, Mg, and K, which can promote mineral precipitation and surface complexation with contaminants [30–32]. In contrast, corn stover and rice husk biochars are predominantly silica-based and may require chemical activation to achieve comparable performance.

Moreover, *Sargassum* biomass is abundant, fast-growing, and does not compete with food crops, making it a more sustainable and scalable feedstock compared to agricultural residues [29,32]. Recent studies have shown that algal biochar can achieve higher adsorption capacities for heavy metals and anions due to its intrinsic functional groups and mesoporous structure.

Interest in iron modification for magnetic biochar is increasing because iron modification of biochar gives magnetic qualities that make it easier to separate the contaminants from water during the adsorption process [29]. Iron modifications to biochar have been introduced through the use of magnetic minerals, particularly iron oxide (Fe_3O_4). This method tackles simple loss and difficult adsorbent recovery during water treatment [31]. Magnetic biochar is a suitable and efficient option for removing pollutants because it alters the physical and chemical characteristics of the adsorbent by introducing magnetic species. It combines magnetic materials' and biochar's beneficial qualities [33].

This research aims to investigate the synthesis and application of a marine algae-derived adsorbent impregnated with iron oxide (Fe_3O_4) for fluoride adsorption. Macroalgae are abundant and renewable biomass sources with unique compositional characteristics, making them suitable for biochar production. The incorporation of iron oxide onto biochar surfaces aims to enhance fluoride adsorption through increased surface activity and magnetic separation properties. This research evaluates the effectiveness of this novel adsorbent and its potential for addressing fluoride contamination in water systems, contributing to sustainable and efficient techniques for water treatment.

2. Materials and Methods

2.1. Biochar Preparation Using Brown Seaweed and Its Iron Modification

Brown seaweed collected from Manora Island, Karachi, Pakistan, was oven-dried for 3 h at 120 °C. After crushing and sieving the dried macroalgae, it was placed in a stainless steel reactor inside the furnace for the production of the biochar at a temperature of 400 °C for 2 h. Then the prepared biochar was modified using 11.1 g of $FeSO_4{\cdot}7H_2O$ and 20 g of $FeCl_3{\cdot}6H_2O$ in 600 mL of deionized water. After boiling the solution at 80 °C, the biochar was filtered and washed three times with ethanol and deionized water and finally dried at 70 °C for 12 h. This methodology was used in our previous research [28,33,34].

2.2. Chemicals and Reagents

A stock solution of fluoride at a concentration of 100 ppm was prepared by dissolving 22.1 mg of sodium fluoride (NaF, 99%) in 100 mL of distilled water. This stock solution was subsequently diluted with deionized water to create standard solutions with fluoride concentrations ranging from 5 to 25 mg/L. The pH of these solutions was adjusted using hydrochloric acid (HCl, 37%) and sodium hydroxide (NaOH, ≥97%, Merck, Darmstadt, Germany). For the modification of biochar, iron sulfate heptahydrate ($FeSO_4{\cdot}7H_2O$, analytical grade, ≥99%, Sigma-Aldrich, Burlington, MA, USA) and iron chloride hexahydrate ($FeCl_3{\cdot}6H_2O$, analytical grade, ≥99%, Sigma-Aldrich) were utilized.

2.3. Analysis

The SPANDS technique and UV spectrophotometer (Perkinelmer, Lamda 365, Springfield, IL, USA) were used to analyze fluoride. All samples were analyzed through standard methods.

2.4. Characterization of Biochar (BC) and Iron Impregnated Biochar (MBC)

To comprehend their function in adsorption, many physicochemical characteristics of the BC and MBC were examined. Both BC and MBC's surface morphology was examined with a JEOL (Tokyo, Japan) scanning electron microscope (SEM). With the aid of an

automated nitrogen adsorption analyzer (Micromeritics ASAP 2020N, Norcross, GA, USA), the Brunauer–Emmett–Teller (BET) surface area was determined. Additionally, energy-dispersive X-ray spectroscopy (EDS) was used to analyze the elemental composition of the biochar and iron-impregnated biochar. A Shimadzu FTIR Spectrometer, which operates in the 400–4000 cm^{-1} wavelength range with a resolution of 8.0 cm^{-1}, was used to collect the infrared spectra of the BC and MBC.

2.5. Batch Experiments

Batch adsorption experiments were executed in 100 mL Erlenmeyer flasks containing fluoride solutions to identify the optimal conditions for the adsorption of fluoride. The experiments varied in terms of initial fluoride concentration (5 to 25 mg/L), contact time (30 to 150 min), pH (2 to 10), and adsorbent dosage (10 to 60 mg). The fluoride solutions were stirred at 180 rpm at a room temperature of 35 °C. After equilibrium was reached, all samples were filtered using 0.45 µm syringe filters. The following formulas were used to determine the adsorption capacity and fluoride adsorption efficiency [35–37]:

$$\text{Fluoride removal efficiency } (\%) = \frac{(C_i - C_e)}{C_i} \times 100 \quad (1)$$

$$q_e = \frac{(C_i - C_e)}{m} \times V \quad (2)$$

where C_i is the initial concentration of fluoride (mg/L), C_e is the equilibrium fluoride concentration (mg/L), q_e is fluoride adsorption capacity (mgg^{-1}), m is the mass of adsorbent (g), and V is the volume of solution (L).

2.6. Isotherm Modelling

The efficacy of the adsorption mechanism for a batch adsorptive equilibrium is well understood by introducing the adsorption isotherm models. This model also governs the determination of instrumental designs of the adsorption mechanism to achieve a more excellent value and effectiveness in the case of the separation of fluoride content from wastewater. In the current study on the batch adsorption mechanism, different kinds of isotherm studies are considered, such as the Langmuir and Freundlich models.

Endorsement of the first isotherm, i.e., the Langmuir model, deals with the adsorbate molecules having only a single layer that is adsorbed on the surface of the porous adsorbent molecule. This model infers the existence of a limited and adequate number of porous adsorption sites having comparable energies and independent of restoring capacity and removal ability.

Secondly, the removal efficiency relating to the heterogeneous adsorbent surface is assessed in the Freundlich adsorption isotherm. Furthermore, it demonstrates the surface heterogeneity as well as the multilayer formation of the adsorbent.

The mathematical equations of the Langmuir and Freundlich models can be defined as (Equations (3) and (4)):

$$\frac{C_e}{q_e} = \frac{1}{q_m h_L} + \frac{C_e}{q_m} \quad (3)$$

$$\log q_e = \log C_e \left(\frac{1}{f}\right) + \log h_F \quad (4)$$

where q_m defines the maximum adsorption capacity (mg/g), h_L and h_F are defined as Langmuir and Freundlich constants, and 1/f is the heterogeneity factor.

2.7. Kinetic Models

Adsorption kinetics can be elucidated as the study of the prediction of adsorption uptake over time, either at a fixed concentration or throughout a continuous process. The study details ideal circumstances, adsorbate diffusion in pores, the sorption process, and the rate-controlling step. The prosecution and implementation of three kinetic models are considered to stimulate the predicted data: a model of intraparticle diffusion, pseudo-first-order kinetics, and pseudo-second-order kinetics. It is acceptable to describe the process of bioaccumulation of solids or liquid particles using a pseudo-first-order model. It claims that the alterations in concentration are time-dependent on a quantitative level.

The intraparticle diffusion model specifies the rate-controlling phase of the sorption system, which is a crucial kinetics-based stage. Three steps are involved in aqueous dye adsorption onto the surface of the adsorbent. Molecular diffusion moves Sorbate particles from a bulk phase to an external adsorbent surface. This procedure is often referred to as outward diffusion or film. The second stage consists of the distribution and movement of sorbate particles from the surface of the adsorbent to the interior porous adsorption sites. The third phase involves the chemisorption of sorbate particles from interior locations to internal pores. The most sluggish stage, the rate-controlling phase, regulates the rate of the entire biosorption method.

The mathematical equations of pseudo-first and second-order- and infraparticle diffusion kinetics models can be expressed as:

$$\ln(q_e - q_t) = \ln q_e h_1 t \quad (5)$$

$$\frac{t}{q_t} = \frac{t}{q_e} + \frac{1}{h_2 q_e^2} \quad (6)$$

$$q_t = C + bt^{0.5} \quad (7)$$

where h_1 (min^{-1}) and h_2 (g mg^{-1} min^{-1}) are the coefficients of pseudo first and second orders, C is the plot's intercept, and b represents the constant of infraparticle diffusion (mg g^{-1} min^{-1}).

2.8. Desorption Study

After the adsorption equilibrium was reached, the adsorbent within the sample solution was filtered using a 0.45 µm Whatman filter. The adsorbed fluoride was then desorbed from the adsorbent using a 0.1 mol/L NaOH solution. The adsorbent was then collected using a 0.45 µm Whatman filter and underwent several washes with deionized water to guarantee complete removal and dried for 2 h at 105 °C.

3. Results and Discussion

3.1. Characterization

3.1.1. Surface Morphology of the Biochar

The surface morphology of BC and MBC was examined through SEM analysis. The unmodified biochar displayed its typical structural traits, including an irregular yet smooth surface, as illustrated in Figure 1a, consistent with findings reported in earlier studies [37,38], in which the authors described the structure of the biochar as having a relatively low surface area and limited interaction with adsorbates. In contrast, impregnating the biochar with $FeSO_4$ and $FeCl_3$ significantly altered its surface. As seen in Figure 1b, the surface of the MBC became rougher and more heterogeneous, indicating the formation of clusters due to the iron deposition compounds onto the biochar. This occurrence was explained as a result of magnetic forces combined with the effects of surface tension, as described by [39],

who reported that iron-modified biochar exhibits increased surface heterogeneity, which could enhance the material's ability to interact with contaminants.

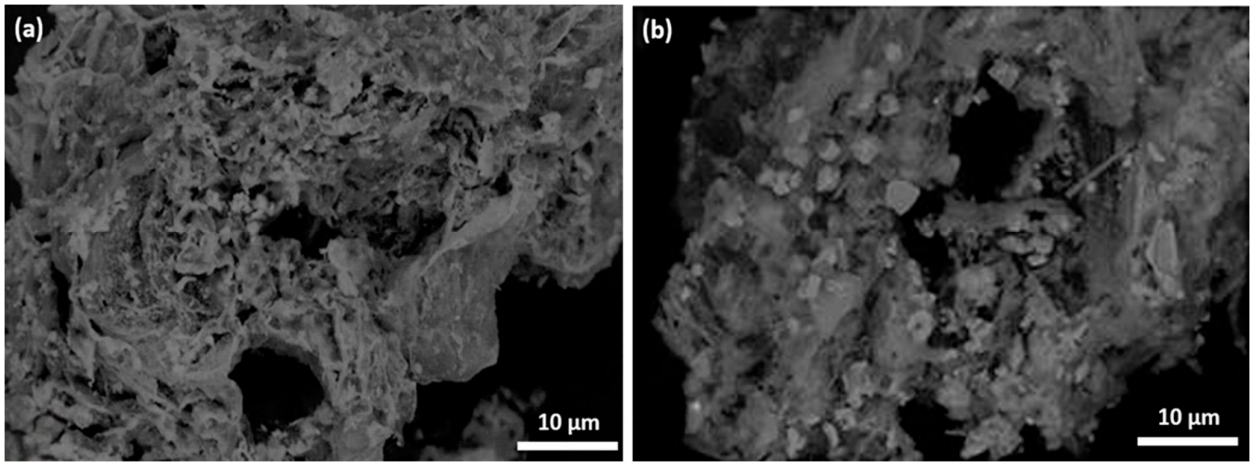

Figure 1. SEM images of the biochar (**a**) before and (**b**) after iron modification.

The surface area of BC and MBC was determined using Brunauer–Emmett–Teller (BET) analysis. The findings indicated that the unmodified biochar possessed a surface area of 0.52 m^2/g. In contrast, the iron-modified biochar demonstrated a markedly enhanced surface area of 168.29 m^2/g. Additionally, the pore volume of the unmodified biochar was measured at 0.013 cm^3/g, which significantly increased to 0.746 cm^3/g following iron modification.

3.1.2. Elemental Composition of the Biochar

Energy-dispersive X-ray spectroscopy (EDS) was employed to examine the elemental analysis of both raw and iron oxide-impregnated biochar. The findings revealed that the surfaces of both types of biochar included various elements. This diversity in surface composition suggests a high degree of stability, attributable to the inherent properties of biochar. Additionally, it revealed that the most prevalent elements in raw biochar were carbon (33.8%) and oxygen (49.93%). Significant levels of oxygen, carbon, sulfur, phosphorus, sodium, chlorine, and iron were the primary elements identified in the MBC. The percentages of these elements' atomic and compound weights in the raw and iron-impregnated adsorbents are summarized below in Table 1. However, iron modification raised the percentages of carbon and iron while decreasing the percentage of oxygen, demonstrating iron oxide modification on the biochar surface, which also corroborated the observations of [38], highlighting that iron impregnation increases the carbon content due to the deposition of iron oxide on biochar. Nevertheless, the percentages of calcium, phosphorus, magnesium, sodium, potassium, silicon, and aluminum also decreased with the iron-treated biochar, as observed before by [40].

The significant increase in iron content (from undetectable to 32.25% atomic weight) is a direct result of the successful co-precipitation of Fe_3O_4 nanoparticles onto the biochar surface, which was confirmed by new Fe–O vibrational peaks in the FTIR spectrum. This iron impregnation is the primary reason for the enhanced fluoride adsorption, as Fe_3O_4 provides abundant active sites for chemisorption via ligand exchange, explaining the high adsorption capacity and the excellent fit to the pseudo-second-order kinetic model. The apparent increase in carbon content and decrease in oxygen content are attributed to the deposition of heavy iron oxide particles (a "dilution effect" on the EDS signal) and the consumption of surface oxygen functional groups during iron oxide formation, respectively, corroborating findings from reference [38,41]. The reduction in other ash elements (Ca,

Mg, K, etc.) is similar due to this dilution effect, as the iron dominates the elemental composition.

Table 1. Elemental analysis of BC and MBC using EDS.

		Elements												Total (%)
		C	O	Mg	K	Na	Si	N	Al	Cl	P	Ca	S	Fe	
BC	Atomic weight (%)	37.85	52.24	1.13	1.22	0.59	2.48	-	1.47	-	1.44	1.58	-	-	100
	Compound weight (%)	33.79	49.93	1.40	1.84	1.34	4.66	-	2.35	-	1.96	1.58	-	-	100
MBC	Atomic weight (%)	40.52	24.46	0.22	-	0.83	1.03	0.09	-	0.27	-	-	0.33	32.25	100
	Compound weight (%)	41.93	16.25	0.36	-	1.54	2.28	0.33	-	1.40	-	-	0.86	35.05	100

These elemental changes are fundamental to the material's superior performance. The introduced Fe_3O_4 nanoparticles are the main drivers for fluoride removal, enabling strong chemical binding. Furthermore, the FTIR analysis shows a significant increase in the intensity of the O–H absorption band in MBC, indicating that the iron modification creates a new population of highly reactive surface hydroxyl groups, which are the crucial functional groups for the ligand exchange reaction with fluoride ions.

3.1.3. Functional Groups Analysis of BC and MBC Using FTIR

As illustrated in Figure 2, the functional groups available on the BC and MBC surfaces were determined using FTIR analysis. The spectral peaks for BC and MBC showed similarities in terms of wavenumbers. Peaks near 1782 cm^{-1} and 1627 cm^{-1} were attributed to C=O and C–O groups, representing the existence of carboxyl and aromatic compounds [39].

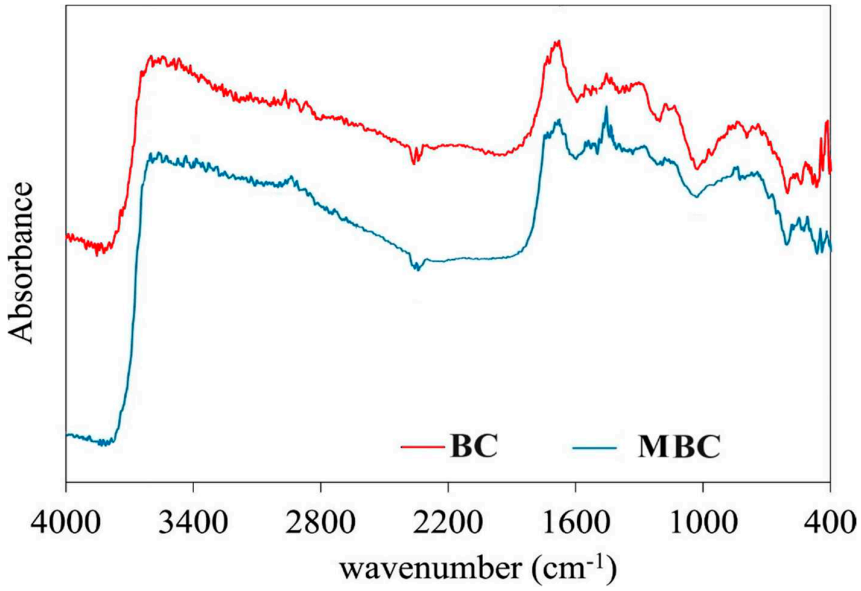

Figure 2. FTIR spectrum of macroalgae BC and MBC.

In the case of MBC, a significant increase in the intensity of the O–H absorption band was noted, suggesting a high concentration of hydroxyl groups due to the integration of iron. Additionally, new peaks at 620 cm^{-1} and 817 cm^{-1} were identified, which correspond to Fe–O vibrations associated with iron oxides like Fe_2O_3 and Fe_3O_4. These hydroxyl groups enhance the hydrophilicity and reactivity of the biochar surface, thereby improving its adsorption capacity. Similar observations have been reported in studies where iron modification significantly increased O–H functional group signals in FTIR spectra [42].

Overall, the FTIR results indicate that the chemically modified biochar notably altered the biochar's surface properties. The new active sites were formed by increasing the intensity of the functional groups, which could enhance the biochar's potential for fluoride adsorption.

3.2. Fluoride Removal Batch Experiments

3.2.1. Influence of Fluoride Initial Concentration

The study investigated the impact of varying initial fluoride concentrations on the adsorption process, observing significant changes in adsorption capacity. Under optimal conditions (including stirring time, pH, and adsorbent dosage), the adsorption capacity was enhanced substantially as the fluoride content rose from 5 to 30 mg/L. Specifically, the capacity surged from 2.4 to 21.3 mg/g, as illustrated in Figure 3. Fluoride adsorption efficiency was achieved at 85.24% at the highest tested fluoride concentration of 30 mg/L.

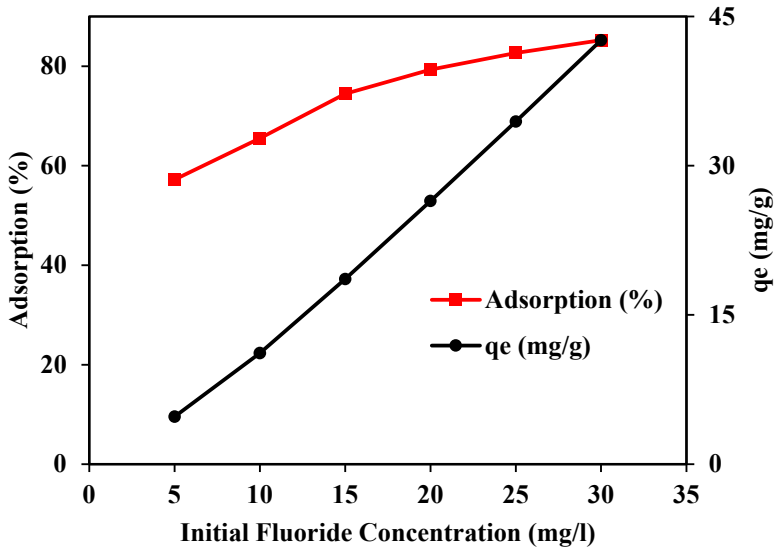

Figure 3. Influence of fluoride levels on the adsorption efficiency of an iron-impregnated adsorbent.

This observed trend supports the principle that high concentrations of adsorbate tend to enhance the capacity of the adsorbent. This phenomenon occurs because a greater concentration of adsorbate molecules results in more frequent interactions between the adsorbate and the functional groups on the adsorbent, thereby enhancing the overall adsorption process [27].

3.2.2. Influence of Contact Time

Under optimal conditions (fluoride concentration: 25 mg/L, pH: 4, adsorbent dosage: 60 mg), the influence of contact time on fluoride adsorption by iron-modified biochar was studied. The fluoride adsorption capacity increased from 12.1 mg/g to 17.2 mg/g as contact time extended from 30 to 150 min. The highest fluoride removal efficiency of 82.4% was obtained at 150 min. Initially, the adsorption efficiency rose rapidly from 58.3% to 76.8% within the first 90 min and then increased gradually up to 150 min (Figure 4). This rapid initial adsorption was due to the abundance of available adsorption sites and the high fluoride concentration, which created a strong driving force for fluoride removal. As the process continued, the rate of fluoride uptake slowed significantly. This deceleration was attributed to the decreased accessibility of adsorption sites and the lower fluoride concentration in the solution, which weakened the concentration gradient driving the adsorption process [43].

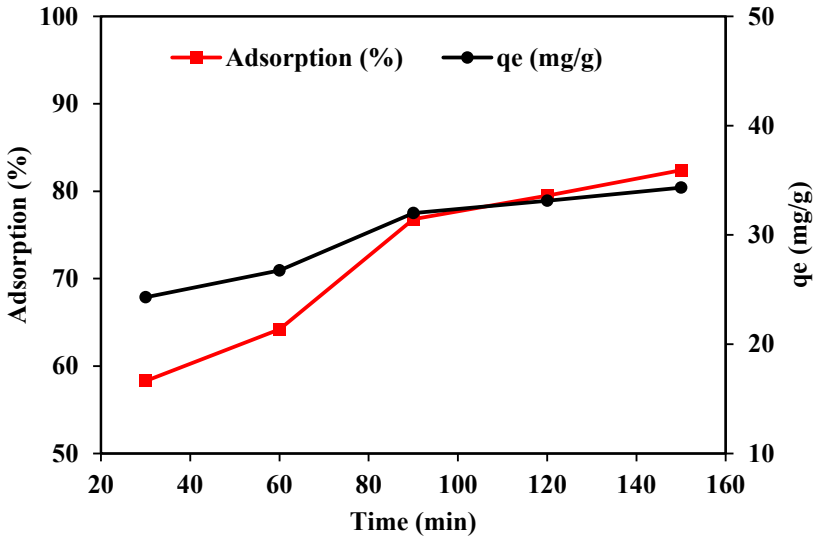

Figure 4. Impact of contact time on the adsorption capacity of the iron-modified adsorbent (adsorbent dosage: 60 mg/L, fluoride concentration: 25 mg/L, pH: 4, temperature: 35 °C).

3.2.3. Influence of Adsorbent Dose

The influence of adsorbent dose on fluoride adsorption capacity was examined using iron-modified biochar. The highest fluoride adsorption efficiency of iron impregnated biochar (MBC) reached 90.2% at an adsorbent dosage of 60 mg. The fluoride adsorption efficiency increased from 50.8% to 90.2% with increasing adsorbent dosage from 10 to 60 mg, as shown in Figure 5. Higher adsorbent dosages probably result in more active binding sites being available, which boosts efficiency. Moreover, the adsorption capacity of fluoride dropped from 101.6 to 30 mg/g within the given solid/liquid ratio range. The decrease in fluoride concentration in the single solution and on the WMP surface can be ascribed to the disturbance of the flux and concentration gradient. Therefore, considering removal efficiency and economic factors, the optimal adsorbent dose of WMP for fluoride adsorption was selected at 60 mg.

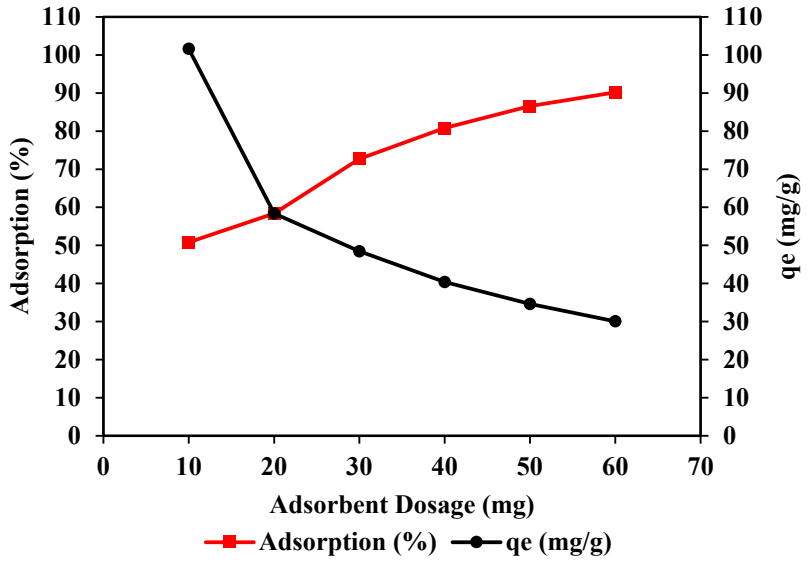

Figure 5. Impact of adsorbent dose on the adsorption capacity of the iron-modified adsorbent (contact time: 150 min, fluoride concentration: 25 mg/L, pH: 4, and temperature: 35 °C).

3.2.4. Effect of pH

Another strong factor, which depends on adsorption, is pH. Figure 6 illustrates that the highest fluoride adsorption capacity was attained at the lowest pH. As the pH increased, the adsorption efficiency decreased. Nevertheless, the removal efficiency drastically decreased from 84.24 to 66.91% at a pH of 6. But there was not much difference observed in the adsorption efficiency between the pH of 2 and 4. When the pH is lower, there are more H+ ions present. These ions help in the hydroxylation process, which makes the adsorbent sites more attractive to fluoride ions. As a result, the efficiency of fluoride adsorption increases. This phenomenon is also supported by the findings of recent studies [43], which emphasize the importance of protonation and the role of H^+ ions in promoting the interaction between fluoride ions and the adsorbent surface. However, at higher pH, the surface became negatively charged and showed the repulsion between fluoride ions and the iron-modified adsorbent, which led to a reduction in adsorption efficiency, and a similar trend was also observed by [27,44,45], who observed that at pH values above 5, the fluoride adsorption capacity of iron-modified adsorbents sharply decreased, attributed to the electrostatic repulsion between the adsorbent surface and the F^- ions. Additionally, the high concentration of OH^- ions in alkaline conditions can lead to the formation of hydroxylated species, which can further reduce the availability of active sites for fluoride adsorption.

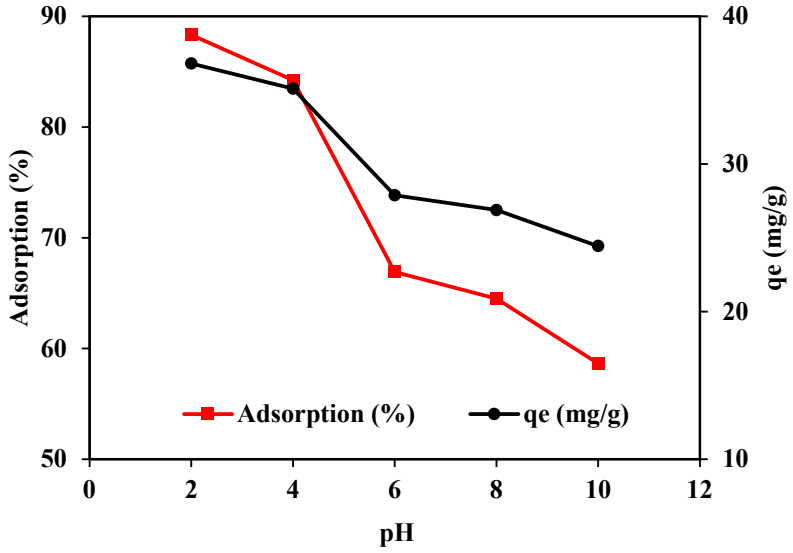

Figure 6. Influence of pH on the adsorption efficiency of the macroalgae-derived adsorbent modified with iron (contact time: 150 min, fluoride concentration: 25 mg/L, adsorbent dosage: 60 mg, and temperature: 35 °C).

3.3. Isotherm Modeling

It is essential to comprehend the interactions between contaminants and the surface of biochar. Equilibrium adsorption by biochars has been analyzed using various isotherm models. However, in this study, Langmuir and Freundlich isotherms were employed to evaluate the fluoride adsorption behavior on macroalgae-derived biochar impregnated with iron oxide. The data are presented in Figure 7, and the associated parameters are shown in Table 2.

On the homogeneous surface of an adsorbent, the Langmuir isotherm presumes a single molecular layer adsorption process. This implies that a site cannot be used for additional adsorption after a molecule has occupied it. With a strong correlation coefficient (R^2 = 0.998) and the highest removal capacity (q_m) of 3.41 mg/g, the Langmuir isotherm was found to match the data better. This indicates that the adsorption process

forms a uniform, irreversible monolayer of molecules with consistent adsorption energy across the surface [46]. Furthermore, [40] explored the role of surface functional groups and their effect on adsorption by biochar. In their study, they found that the interaction between fluoride ions and biochar surfaces modified with iron oxide resulted in a higher adsorption capacity, consistent with the Langmuir isotherm's prediction of a monolayer adsorption process.

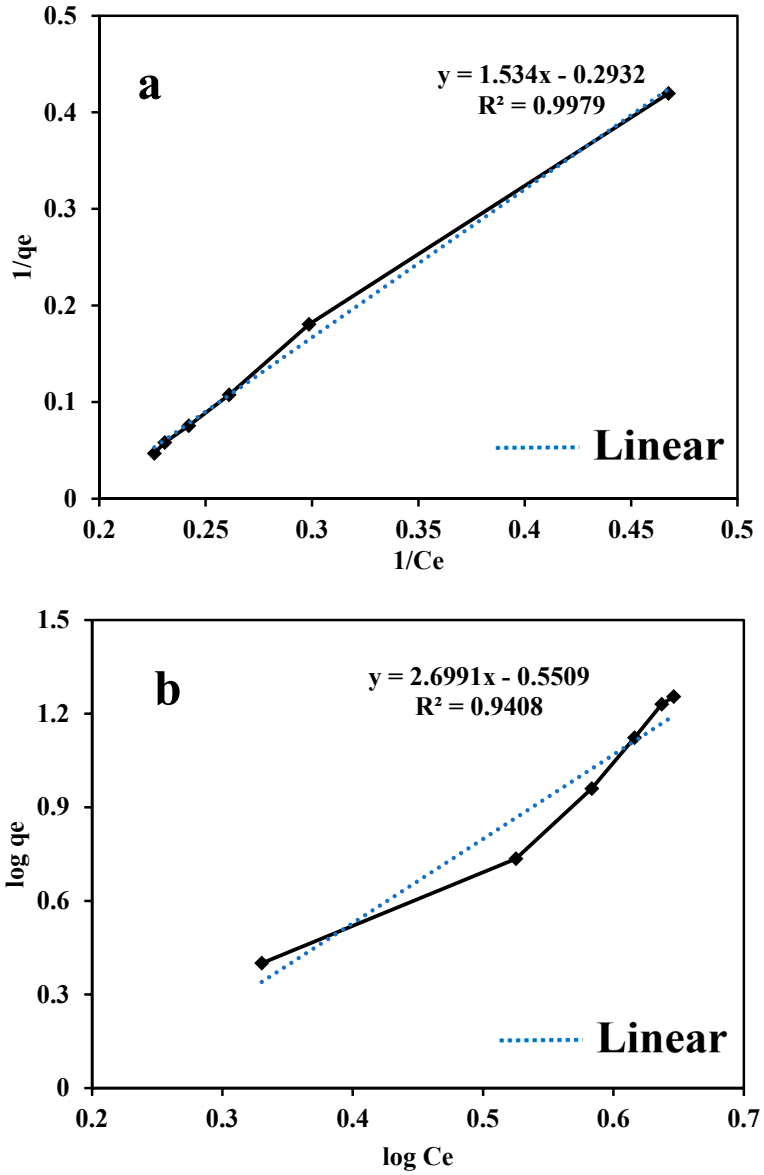

Figure 7. Linear graph of (**a**) the Langmuir and (**b**) Freundlich isotherm models.

In contrast, this model describes adsorption on a heterogeneous surface, typically involving chemical bonding. It accounts for varying adsorption energies and sites. The study authors found a lower correlation coefficient (R^2 = 0.941) for the Freundlich model, suggesting it was less effective than the Langmuir isotherm model in explaining the adsorption behavior [40].

The findings, summarized in Table 2 and demonstrated in Figure 7a,b, reveal that the Langmuir isotherm presents a better fit, indicating its effectiveness in describing fluoride adsorption on iron-modified biochar. The Langmuir isotherm indicates that the adsorption process forms a uniform, irreversible monolayer of molecules, with consistent adsorption energy across the surface.

Table 2. Fluoride adsorption isotherms and kinetics using macroalgae-derived biochar impregnated with iron oxides.

		Parameters	Units	Values
Isotherms	Langmuir Isotherm	q_m	mgg^{-1}	3.41
		h_L	Lmg^{-1}	0.2
		R^2	-	0.998
	Freundlich Isotherm	f	-	0.4
		h_F	$(mgg^{-1})\ (Lmg^{-1})^{1/n}$	3.55
		R^2	-	0.941
Kinetics	Pseudo-first-order kinetics	h_1	min^{-1}	0.000242
		q_e	mgg^{-1}	25.2
		R^2	-	0.89
	Pseudo-second-order kinetics	h_2	$(g\ mg^{-1}min^{-1})$	0.003
		q_e	mgg^{-1}	19.61
		R^2	-	0.994
	Infraparticle Diffusion Kinetics	q_t	mgg^{-1}	12.1
		B	$g/mg^{-1}min^{-0.5}$	0.8
		C	-	7.74
		R^2	-	0.95

3.4. Adsorption Kinetics

Adsorption kinetics studies aim to analyze how fluoride molecules interact with iron-modified biochar over time and to uncover the mechanisms driving this adsorption process [46]. To achieve this, three well-known kinetic models were evaluated: the pseudo-first-order, pseudo-second-order, and intraparticle diffusion kinetics.

The pseudo-first-order model states that the rate of adsorption is determined by the difference between the saturation capacity of the adsorbent and the concentration of the adsorbate in the solution. Nonetheless, the pseudo-second-order kinetic model suggests that chemical adsorption probably governed the process, which includes interactions like bonding between the adsorbent and the adsorbate [30,35,36]. Last but not least, the intraparticle diffusion model examines how adsorbate molecules move into the interior structure of the adsorbent particles from the solution phase, affecting the total adsorption rate [30,35,36].

The study's findings, summarized in Table 2, compared the model parameters and evaluated their effectiveness using the correlation coefficient (R^2). The findings, illustrated in Figure 8a–c, showed that the pseudo-first-order kinetic model had the lowest R^2 value, making it unsuitable for predicting fluoride adsorption kinetics. Conversely, the pseudo-second-order kinetics had the highest correlation (R^2 = 0.9943), indicating that chemisorption dominated the process due to strong chemical interactions between the functional groups of the adsorbent and adsorbate.

Additionally, the intraparticle diffusion model also demonstrated a relatively strong fit with an R^2 value of 0.9524. The linear relationship between fluoride content and the square root of time further suggested that intraparticle diffusion is crucial in controlling the adsorption process. The adsorption kinetics of fluoride on iron-modified biochar are most effectively explained by pseudo-second-order and intraparticle diffusion kinetics, and these

results align with earlier research [47], the authors of which concluded that chemisorption and intraparticle diffusion play significant roles in fluoride adsorption.

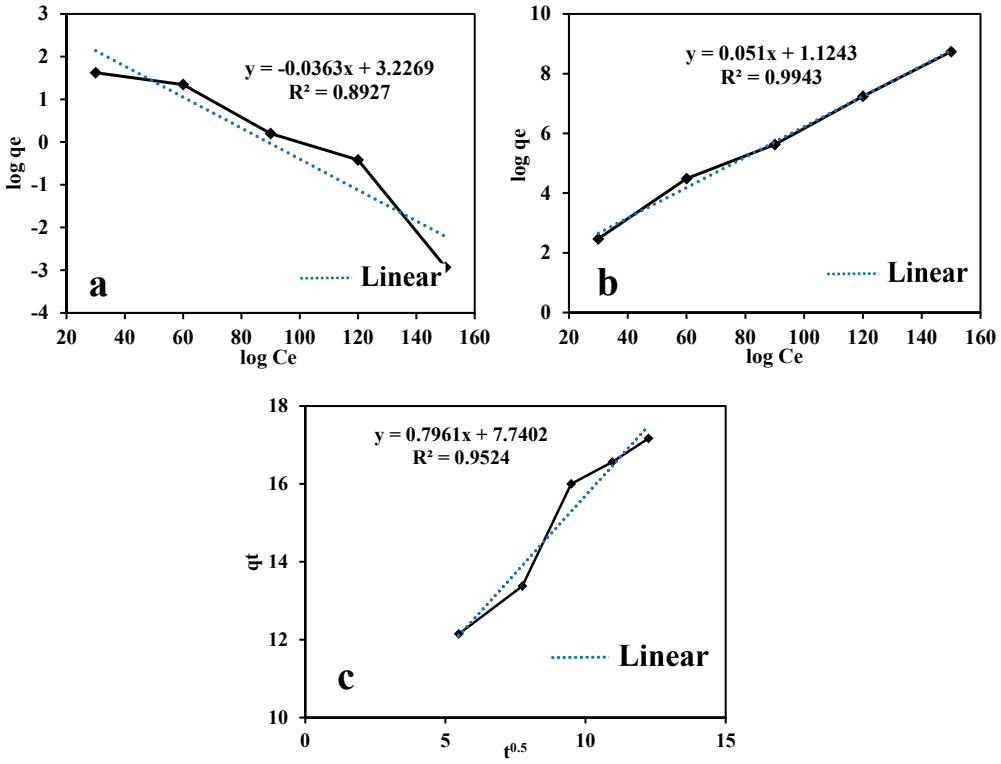

Figure 8. Linearized graphs of (**a**) first-order kinetics (**b**) second-order kinetics (**c**) Infraparticle diffusion kinetics.

3.5. Comparison of the Fluoride Adsorption Efficiencies of Different Adsorbents

A summary of previous research on the adsorption of fluoride via various adsorbents is given in Table 3. Notably, a large number of these capacities were measured at equilibrium times between 60 to 200 min in solutions with pH levels ranging from slightly acidic to neutral (1–7). Regarding arsenic adsorption kinetics, Fe-BC biochar is unique and expresses quick removal within 1.5 h. Additionally, it shows a good capacity for adsorbing arsenic at pH 6, 0.25 mg/L of the initial arsenic concentration. It also shows that the majority of kinetics reported the following pseudo-second order kinetics.

Table 3. Comparison of the adsorption of fluoride using macroalgae-derived iron-modified biochar with other adsorbents.

Adsorbent Materials	Adsorption Efficiency/ Capacity q_m (mg/g)	Operational Conditions	References
Moringa oleifera leaves	1.14 mg/g	pH = 1, fluoride concentration = 2 mg/L, adsorbent dosage = 250 mg, contact time = 150 min	[24]
Dunaliella salina	98.22%	pH=7, temperature = 42.50 °C, fluoride concentration = 50 mg/L, contact time = 40 min, adsorbent dosage = 0.6 g/L	[25]
Blue–green algae, *Phormidium* sp.	60%	Fluoride concentration = 3 mg/L, pH = 4.5, contact time = 90 hrs, adsorbent dosage = 4.5 g	[26]
Waste marble powder (WMP)	1.165 mg/g, 97.13%	pH = 6, fluoride concentration = 6 mg/L, dosage = 500 mg, contact time = 60 min	[16]
Fe_3O_4 modified Rhodophytes (red algae)	96.4 mg/g	pH = 2, fluoride concentration = 60 g/L, adsorbent dosage = 50 g, contact time = 200 min	[27]
Activated carbon of avocado seeds	1.2 mg/g, 86%	pH = 6, Fluoride concentration = 5.2 mg/L, dosage = 190 mg, contact time = 60 min	[28]
Iron oxide magnetic biochar using brown seaweed (Fe-BC)	3.41 mg/g, 90.2%	Fluoride concentration = 30 mg/L, contact time = 150 min, pH = 2, adsorbent dosage = 60 mg	This study

3.6. Desorption Study

Regeneration plays a crucial role in creating cost-effective adsorbents for fluoride adsorption. In this experiment, 0.1 M NaOH was employed as the regenerating means over five cycles. The desorption efficiency gradually declined from 91% during the first cycle to 53% by the fifth cycle, as shown in Figure 9 These results suggest that 0.1 M NaOH is a viable option for regenerating spent biochar, making it a practical choice for industrial and commercial applications.

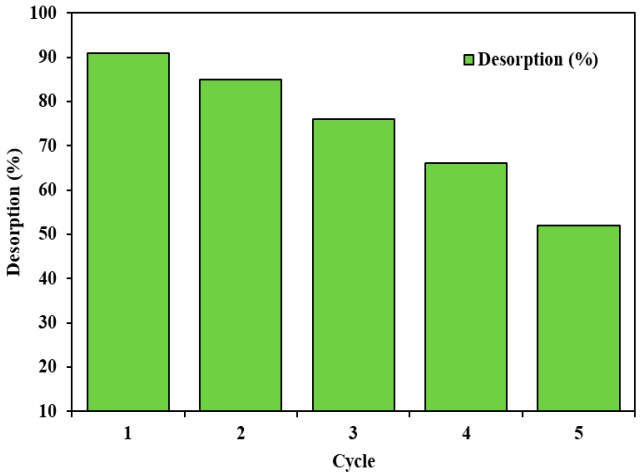

Figure 9. Regeneration efficiency of the iron-modified adsorbent up to the 5 cycles (at an initial fluoride content of 25 mg/L, an adsorbent dosage of 60 mg, and a pH of 4).

4. Conclusions

Magnetic Fe_3O_4 nanoparticles have been successfully added to brown macroalgae charcoal to create a bio-adsorbent that is both economically feasible and biologically sound. This adsorbent is an excellent, economical, highly effective, environmentally friendly, sustainable, and green adsorbing agent that can separate materials quickly when exposed to an external magnetic field. Following modification with Fe_3O_4 particles, the macroalgae-based bio-adsorbent demonstrated a remarkable affinity for the adsorption of harmful fluoride ions from its aqueous solution. Several successful batch sorption tests were carried out to ascertain the equilibrium condition. The use of the magnetic bio-adsorbent for fluoride adsorption from water could be advanced by conducting techno-economic assessments, evaluating the environmental impact, promoting interdisciplinary relationships, optimizing synthesis for increased efficiency, and investigating this study on a large scale for trials. The study was well-established using the Langmuir and Freundlich isotherms that were well-fitted to intraparticle diffusion kinetics and pseudo-second-order kinetics, with a sorption capacity of 3.4 mg/g. For the adsorption of fluoride ions from wastewater and other large-scale applications, MBC was found to be an efficient bio-adsorbent.

Author Contributions: Conceptualization, S.K. and S.K.D.; methodology, S.K. and S.A.K.H.; formal analysis, S.K. and S.K.D.; investigation, S.K.; resources, S.A.K.H.; data curation, S.A.K.H.; writing—original draft preparation, S.K. and S.K.D.; writing—review and editing, S.K. and S.K.D. All authors made equal contributions to this study. All authors have read and agreed to the published version of the manuscript.

Funding: This research received no external funding.

Institutional Review Board Statement: Not applicable.

Informed Consent Statement: Not applicable.

Data Availability Statement: The original contributions presented in this study are included in the article. Further inquiries can be directed to the corresponding author.

Conflicts of Interest: The authors declare no conflicts of interest.

References

1. Maity, J.P.; Vithanage, M.; Kumar, M.; Ghosh, A.; Mohan, D.; Ahmad, A.; Bhattacharya, P. Seven 21st Century Challenges of Arsenic-Fluoride Contamination and Remediation. *Groundw. Sustain. Dev.* **2021**, *12*, 100538. [CrossRef]
2. Vithanage, M.; Bhattacharya, P. Fluoride in Drinking Water: Health Effects and Remediation. In *CO_2 Sequestration, Biofuels and Depollution*; Springer International Publishing Switzerland: Cham, Switzerland, 2015; pp. 105–151. [CrossRef]
3. Kumar, H.; Patel, M.; Mohan, D. Simplified Batch and Fixed-Bed Design System for Efficient and Sustainable Fluoride Removal from Water Using Slow Pyrolyzed Okra Stem and Black Gram Straw Biochars. *ACS Omega* **2019**, *4*, 19513–19525. [CrossRef]
4. Kimambo, V.; Bhattacharya, P.; Mtalo, F.; Mtamba, J.; Ahmad, A. Fluoride Occurrence in Groundwater Systems at Global Scale and Status of Defluoridation—State of the Art. *Groundw. Sustain. Dev.* **2019**, *9*, 100223. [CrossRef]
5. Bundschuh, J.; Maity, J.P.; Mushtaq, S.; Vithanage, M.; Seneweera, S.; Schneider, J.; Bhattacharya, P.; Khan, N.I.; Hamawand, I.; Guilherme, L.R.G.; et al. Medical Geology in the Framework of the Sustainable Development Goals. *Sci. Total Environ.* **2017**, *581–582*, 87–104. [CrossRef]
6. Ali, S.; Fakhri, Y.; Golbini, M.; Thakur, S.K.; Alinejad, A.; Parseh, I.; Shekhar, S.; Bhattacharya, P. Concentration of Fluoride in Groundwater of India: A Systematic Review, Meta-Analysis and Risk Assessment. *Groundw. Sustain. Dev.* **2019**, *9*, 100224. [CrossRef]
7. Ijumulana, J.; Ligate, F.; Irunde, R.; Bhattacharya, P.; Maity, J.P.; Ahmad, A.; Mtalo, F. Spatial Uncertainties in Fluoride Levels and Health Risks in Endemic Fluorotic Regions of Northern Tanzania. *Groundw. Sustain. Dev.* **2021**, *14*, 100618. [CrossRef]
8. Zhu, J.; Zhao, H.; Ni, J. Fluoride Distribution in Electrocoagulation Defluoridation Process. *Sep. Purif. Technol.* **2007**, *56*, 184–191. [CrossRef]
9. Mameri, N.; Yeddou, A.R.; Lounici, H.; Belhocine, D.; Grib, H.; Bariou, B. Defluoridation of Septentrional Sahara Water of North Africa by Electrocoagulation Process Using Bipolar Aluminium Electrodes. *Water Res.* **1998**, *32*, 1604–1612. [CrossRef]
10. Araga, R.; Soni, S.; Sharma, C.S. Fluoride Adsorption from Aqueous Solution Using Activated Carbon Obtained from KOH-Treated Jamun (*Syzygium cumini*) Seed. *J. Environ. Chem. Eng.* **2017**, *5*, 5608–5616. [CrossRef]
11. Zúñiga-Muro, N.M.; Bonilla-Petriciolet, A.; Mendoza-Castillo, D.I.; Reynel-Ávila, H.E.; Tapia-Picazo, J.C. Fluoride Adsorption Properties of Cerium-Containing Bone Char. *J. Fluor. Chem.* **2017**, *197*, 63–73. [CrossRef]
12. Ndiaye, P.I.; Moulin, P.; Dominguez, L.; Millet, J.C.; Charbit, F. Removal of Fluoride from Electronic Industrial Effluentby RO Membrane Separation. *Desalination* **2005**, *173*, 25–32. [CrossRef]
13. Shen, J.; Schäfer, A. Removal of Fluoride and Uranium by Nanofiltration and Reverse Osmosis: A Review. *Chemosphere* **2014**, *117*, 679–691. [CrossRef] [PubMed]
14. Khatibikamal, V.; Torabian, A.; Janpoor, F.; Hoshyaripour, G. Fluoride Removal from Industrial Wastewater Using Electrocoagulation and Its Adsorption Kinetics. *J. Hazard. Mater.* **2010**, *179*, 276–280. [CrossRef] [PubMed]
15. Hu, T.; Zhou, W.; Tang, W. Metal-organic framework-derived diatomic catalysts for environmental remediation: Synthesis, applications and improvement strategies. *Coord. Chem. Rev.* **2025**, *526*, 216357. [CrossRef]
16. Kanwal, S.; Devi, P.; Ahmed, Z.; Qambrani, N.A. Adsorption Isotherm, Kinetic and Thermodynamic Studies for Adsorption of Fluoride on Waste Marble Powder. *Desalination Water Treat.* **2024**, *319*, 100441. [CrossRef]
17. Bordoloi, N.; Goswami, R.; Kumar, M.; Kataki, R. Biosorption of Co (II) from Aqueous Solution Using Algal Biochar: Kinetics and Isotherm Studies. *Bioresour. Technol.* **2017**, *244*, 1465–1469. [CrossRef]
18. Ahmad, M.; Rajapaksha, A.U.; Lim, J.E.; Zhang, M.; Bolan, N.; Mohan, D.; Vithanage, M.; Lee, S.S.; Ok, Y.S. Biochar as a Sorbent for Contaminant Management in Soil and Water: A Review. *Chemosphere* **2014**, *99*, 19–33. [CrossRef]
19. Kloss, S.; Zehetner, F.; Dellantonio, A.; Hamid, R.; Ottner, F.; Liedtke, V.; Schwanninger, M.; Gerzabek, M.H.; Soja, G. Characterization of Slow Pyrolysis Biochars: Effects of Feedstocks and Pyrolysis Temperature on Biochar Properties. *J. Environ. Qual.* **2012**, *41*, 990–1000. [CrossRef]
20. Brewer, C.E.; Schmidt-Rohr, K.; Satrio, J.A.; Brown, R.C. Characterization of Biochar from Fast Pyrolysis and Gasification Systems. *Environ. Prog. Sustain. Energy* **2009**, *28*, 386–396. [CrossRef]
21. Mohan, D.; Kumar, S.; Srivastava, A. Fluoride Removal from Ground Water Using Magnetic and Nonmagnetic Corn Stover Biochars. *Ecol. Eng.* **2014**, *73*, 798–808. [CrossRef]
22. Gandhi, N.; Sirisha, D.; Shekar, K.B.; Asthana, S. Removal of Fluoride from Water and Waste Water by Using Low Cost Adsorbents. *Int. J. Chemtech Res.* **2012**, *4*, 1646–1653.
23. Tarazona-Díaz, M.P.; Viegas, J.; Moldao-Martins, M.; Aguayo, E. Bioactive Compounds from Flesh and By-Product of Fresh-Cut Watermelon Cultivars. *J. Sci. Food Agric.* **2011**, *91*, 805–812. [CrossRef] [PubMed]

24. Kavisri, M.; Abraham, M.; Moovendhan, M. Effective Removal of Fluoride Ions from Aqueous Solution by Marine Microalgae as Natural Biosorbent. *Chemosphere* **2023**, *313*, 137312. [CrossRef]
25. Dan, S.; Chattree, A. Sorption of Fluoride Using Chemically Modified Moringa Oleifera Leaves. *Appl. Water Sci.* **2018**, *8*, 76. [CrossRef]
26. Mittal, Y.; Srivastava, P.; Kumar, N.; Yadav, A.K. Remediation of Fluoride Contaminated Water Using Encapsulated Active Growing Blue-Green Algae, Phormidium Sp. *Environ. Technol. Innov.* **2020**, *19*, 100855. [CrossRef]
27. Hota, A.; Patro, S.G.K.; Panda, S.K.; Khan, M.A.; Hasan, M.A.; Islam, S.; Alsubih, M.; Khan, N.A.; Zahmatkesh, S. Removing Fluoride Ions from Wastewater by Fe3O4 Nanoparticles: Modified Rhodophytes (*Red algae*) as Biochar. *J. Water Process Eng.* **2024**, *58*, 104776. [CrossRef]
28. Tefera, N.; Mulualem, Y.; Fito, J. Adsorption of Fluoride from Aqueous Solution and Groundwater onto Activated Carbon of Avocado Seeds. *Water Conserv. Sci. Eng.* **2020**, *5*, 187–197. [CrossRef]
29. Devrajani, S.K.; Ahmed, Z.; Qambrani, N.A.; Kanwal, S.; Sundaram, U.M.; Mubarak, N.M. Mechanism of Arsenic Removal Using Brown Seaweed Derived Impregnated with Iron Oxide Biochar for Batch and Column Studies. *Sci. Rep.* **2024**, *14*, 18102. [CrossRef]
30. Kumar, G.; Sivagurunathan, P.; Zhen, G.; Kobayashi, T.; Kim, S.-H.; Xu, K. Combined Pretreatment of Electrolysis and Ultra-Sonication towards Enhancing Solubilization and Methane Production from Mixed Microalgae Biomass. *Bioresour. Technol.* **2017**, *245*, 196–200. [CrossRef]
31. Zhou, Y.; Liu, G.; Liu, J.; Xiao, Y.; Wang, T.; Xue, Y. Magnetic Biochar Prepared by Electromagnetic Induction Pyrolysis of Cellulose: Biochar Characterization, Mechanism of Magnetization and Adsorption Removal of Chromium (VI) from Aqueous Solution. *Bioresour. Technol.* **2021**, *337*, 125429. [CrossRef]
32. Wu, F.; Chen, L.; Hu, P.; Zhou, X.; Zhou, H.; Wang, D.; Lu, X.; Mi, B. Comparison of properties, adsorption performance and mechanisms to Cd (II) on lignin-derived biochars under different pyrolysis temperatures by microwave heating. *Environ. Technol. Innova* **2022**, *25*, 102196. [CrossRef]
33. Yi, Y.; Huang, Z.; Lu, B.; Xian, J.; Tsang, E.P.; Cheng, W.; Fang, J.; Fang, Z. Magnetic Biochar for Environmental Remediation: A Review. *Bioresour. Technol.* **2020**, *298*, 122468. [CrossRef]
34. Tomiyasu, H.; Fukutomi, H.; Gordon, G. Kinetics and Mechanism of Ozone Decomposition in Basic Aqueous Solution. *Inorg. Chem.* **1985**, *24*, 2962–2966. [CrossRef]
35. Kołodyńska, D.; Wnętrzak, R.; Leahy, J.J.; Hayes, M.H.B.; Kwapiński, W.; Hubicki, Z. Kinetic and Adsorptive Characterization of Biochar in Metal Ions Removal. *Chem. Eng. J.* **2012**, *197*, 295–305. [CrossRef]
36. Ali, I.; Alharbi, O.M.L.; ALOthman, Z.A.; Alwarthan, A.; Al-Mohaimeed, A.M. Preparation of a Carboxymethylcellulose-Iron Composite for Uptake of Atorvastatin in Water. *Int. J. Biol. Macromol.* **2019**, *132*, 244–253. [CrossRef] [PubMed]
37. Alqadami, A.A.; Wabaidur, S.M.; Jeon, B.-H.; Khan, M.A. Co-Hydrothermal Valorization of Food Waste: Process Optimization, Characterization, and Water Decolorization Application. *Biomass Convers. Biorefinery* **2024**, *14*, 15757–15768. [CrossRef]
38. Ren, J.; Li, N.; Li, L.; An, J.-K.; Zhao, L.; Ren, N.-Q. Granulation and Ferric Oxides Loading Enable Biochar Derived from Cotton Stalk to Remove Phosphate from Water. *Bioresour. Technol.* **2015**, *178*, 119–125. [CrossRef]
39. Hu, X.; Ding, Z.; Zimmerman, A.R.; Wang, S.; Gao, B. Batch and Column Sorption of Arsenic onto Iron-Impregnated Biochar Synthesized through Hydrolysis. *Water Res.* **2015**, *68*, 206–216. [CrossRef]
40. Khanzada, A.K.; Rizwan, M.; Al-Hazmi, H.E.; Majtacz, J.; Kurniawan, T.A.; Mąkinia, J. Removal of Arsenic from Wastewater Using Hydrochar Prepared from Red Macroalgae: Investigating Its Adsorption Efficiency and Mechanism. *Water* **2023**, *15*, 3866. [CrossRef]
41. Deng, S.; Ting, Y.-P. Characterization of PEI-Modified Biomass and Biosorption of Cu(II), Pb(II) and Ni(II). *Water Res.* **2005**, *39*, 2167–2177. [CrossRef]
42. Regmi, P.; Garcia Moscoso, J.L.; Kumar, S.; Cao, X.; Mao, J.; Schafran, G. Removal of Copper and Cadmium from Aqueous Solution Using Switchgrass Biochar Produced via Hydrothermal Carbonization Process. *J. Environ. Manag.* **2012**, *109*, 61–69. [CrossRef]
43. Bhaumik, R.; Mondal, N.K. Adsorption of Fluoride from Aqueous Solution by a New Low-Cost Adsorbent: Thermally and Chemically Activated Coconut Fibre Dust. *Clean. Technol. Environ. Policy* **2015**, *17*, 2157–2172. [CrossRef]
44. Mondal, N.K.; Bhaumik, R.; Sen, K.; Debnath, P. Adsorption of Fluoride in Aqueous Solutions Using Saline Water Algae (*Rhodophyta* Sp.): An Insight into Isotherm, Kinetics, Thermodynamics and Optimization Studies. *Model. Earth Syst. Environ.* **2022**, *8*, 3507–3521. [CrossRef]
45. Agarwal, S.; Tyagi, I.; Gupta, V.K.; Dehghani, M.H.; Jaafari, J.; Balarak, D.; Asif, M. Rapid Removal of Noxious Nickel (II) Using Novel γ-Alumina Nanoparticles and Multiwalled Carbon Nanotubes: Kinetic and Isotherm Studies. *J. Mol. Liq.* **2016**, *224*, 618–623. [CrossRef]

46. Mohammadnia, M.; Naghizadeh, A. Surveying of Kinetics, Thermodynamic, and Isotherm Processes of Fluoride Removal from Aqueous Solutions Using Graphene Oxide Nano Particles. *J. Birjand Univ. Med. Sci.* **2016**, *23*, 29–43.
47. Sadhu, M.; Bhattacharya, P.; Vithanage, M.; Padmaja Sudhakar, P. Adsorptive Removal of Fluoride Using Biochar—A Potential Application in Drinking Water Treatment. *Sep. Purif. Technol.* **2021**, *278*, 119106. [CrossRef]